Energetics and Dynamics of a Cyclic Oligosaccharide Molecule in a Confined Protein Pore Environment. A Molecular Dynamics Study

Ignat Yu. Shilov and Maria G. Kurnikova*

Chemistry Department, Marquette University, Milwaukee, Wisconsin 53201-1881

Received: February 11, 2003; In Final Form: April 9, 2003

Interaction between a transmembrane pore protein α-hemolysin and a cyclic oligosaccharide *β*-cyclodextrin results in a system that can be viewed from several different perspectives—as an ion channel modified by a noncovalent adapter, thus providing a pivotal building block for the novel single molecule sensor devices, as a model protein−carbohydrate complex, whose structural, dynamical and energetic properties can be helpful in understanding the mechanisms of protein−carbohydrate recognition in biological systems, and as an example of a self-assembling supramolecular system. The detailed understanding of mechanisms of intermolecular interactions in such complexes is, therefore, of wide interest. We have performed a set of molecular dynamics (MD) simulations (20 ns of total reported simulation time) of a *β*-cyclodextrin (*β*CD) molecule confined inside the lumen of the α-hemolysin channel (αHL). For comparison, the 8 ns dynamics of a free *β*CD in bulk aqueous solution was also performed. A detailed analysis of the interaction energetics and conformational flexibility of *β*CD inside the water−protein channel and in water is provided. The intra- and intermolecular hydrogen bonding in the complex and in aqueous solution is elucidated and implications of the confined environment on the dynamics of the cyclodextrin molecule are discussed. We have found that contributions to the binding energy due to the nonpolar solvation and the van der Waals interactions between α-hemolysin and *β*-cyclodextrin are favorable for binding. The equilibrated configurations with *β*CD residing in the vicinity of Met113 residue of αHL protein and with wider rim oriented toward the trans side of the membrane are the most favorable in terms of both interaction and binding energies. This result is in accord with the previous suggestion based on the indirect experimental observations. The formation of the complex is characterized by van der Waals contacts with Met113, Thr115, and Thr145 residues and electrostatic interactions with Glu111 and Lys147. The hydrogen-bonding pattern comprises a few direct bonds with Thr115, Thr145 and several water-mediated hydrogen bonds with Thr115, Thr117, Thr145, and Lys147. Mutation of these residues in addition to Met113, which has already been studied systematically, is expected to alter the binding affinity to *β*CD. Conformational flexibility of the macroring of *β*CD is considerably reduced in the confined environment of the channel. The conformational motion of side groups of α-hemolysin at the binding site is also affected by the presence of *β*CD.

1. Introduction

The structure and thermodynamics of protein−carbohydrate complexes[1−4] have attracted a great attention of scientific community after discovery of new biological roles played by oligosaccharides and carbohydrate binding proteins.[5−7] It was found that interactions between lectins and oligosaccharides mediate cell−cell recognition and, therefore, are involved in such important biological phenomena as fertilization, bacterial infection, inflammatory processes, and cell growth. Interfering with the protein−carbohydrate recognition by modified oligosaccharides has been claimed promising for the therapy of bacterial diseases[8] and cancer.[9] Carbohydrate-binding proteins with other biological functions can be found among enzymes, antibodies, membrane transport proteins, and bacterial periplasmic binding proteins.[3] However, understanding driving forces responsible for the protein−carbohydrate specificity, which is important, e.g., for successful carbohydrate-based drug design, is far from completeness.[1,10−12] In this work, we use molecular dynamics to predict the structure of the α-hemolysin−*β*-cyclodextrin complex and to provide understanding of the cyclodextrin dynamics inside the protein pore in which direct protein−carbohydrate interactions play an important role.

β-Cyclodextrin (*β*CD) belongs to the family of cyclodextrins, cyclic oligomers composed of α-D-glucose units,[13] able to form host−guest complexes with a variety of organic molecules.[14] Due to their ability to form inclusion complexes and also because they are nontoxic and rather inexpensive seminatural products, cyclodextrins are widely utilized in pharmaceutical, food, and cosmetic industries.[15] Although cyclodextrins are physiologically neutral, and no evidence of their participation in cell−cell recognition has been obtained, several examples of crystal and solution structures of protein−*β*CD complexes have been reported recently,[16−20] providing new insights into the structural basis of protein−carbohydrate interactions.

In a series of electrophysiological studies, Bayley and coworkers[21,22] have discovered that *β*CD is able to lodge in the interior of α-hemolysin (αHL) protein pore, resulting in altered conductance and charge selectivity of the channel. What is more interesting, *β*CD bound inside the channel protein preserved its ability to host−guest complexation,[23,24] which revealed itself in additional current blockades. This made the αHL pore a stochastic sensor able to detect a single molecule of analyte by

* Corresponding author. Address after July 2003: Chemistry Department, Carnegie Mellon University, Pittsburgh PA 15213. E-mail: maria.kurnikova@marquette.edu.

10.1021/jp034359w CCC: $25.00
Published on Web 06/26/2003

measuring ionic currents flowing through the channel. On the basis of single-channel recordings combined with mutagenesis data, Bayley and co-workers suggested that βCD binds to αHL at a single site;[21,25] they also suggested a simple kinetic scheme of bimolecular reaction between the βCD and the αHL molecules. However, it is evident that on the atomic level the process of αHL−βCD interaction is far more complicated and involves several steps: entering the channel, diffusion to the binding site (or sites), noncovalent binding, dissociation, and diffusion to the exit of the channel. The nature of binding and the structure of the complex were not clearly elucidated by experimental results. Neither X-ray diffraction nor NMR methods, which can, in principle, provide more direct experimental information about the molecular structure, have been applied to the αHL−βCD complex.

Molecular dynamics (MD) modeling is able to shed light onto mechanisms of biomolecular dynamics and recognition[26] and provide the structural and dynamical information on the supramolecular systems. With ever increasing computational power, simulations of complex biomolecular systems have become feasible. Large-scale computational studies of systems containing tens of thousands of atoms, including simulations of ion channels[27,28] on the time scale of 1−10 ns, have been reported recently. Computer simulations of somewhat smaller globular proteins and peptides on the substantially longer time scales of up to 1 ms have also become a reality.[29,30] However, only a few computational studies on protein−carbohydrate interactions have already been reported.[31−38] On the contrary, applications of computational chemistry to cyclodextrins with their derivatives have a longer history and comprise more than 200 publications.[39] Some of these studies are concerned with conformational analysis of βCD[40−43] and its interaction with water in crystal[44] and solution.[45] However, the majority of works focused on structural and energetic features of host−guest interactions.[46−50] The present MD study is the first computer simulation of interaction between a protein and a cyclodextrin. Furthermore, this is the first computer modeling of a cyclodextrin taking part in host−guest complexation, where in contrast to previous studies, it acts not as a host but rather as a guest. In this complex, the confined environment created by the protein host influences the dynamics of the cyclodextrin molecule.

The large-scale equilibrium molecular dynamics simulations of β-cyclodextrin interacting with the interior of the ion channel formed by α-hemolysin protein presented in this paper provide molecular details of how the confined pore environment influences diffusion, binding properties, and conformational dynamics of the βCD molecule. The total length of the simulations reported in the paper exceeds 20 ns. Although the overall residence time of the βCD molecule inside the protein pore lumen is much longer, on the order of 1 ms, the local relaxation of the protein and the guest molecule placed in one mutual configuration occurs on the time scale less than 1 ns. The overall diffusion process can, therefore, be viewed as a quasiadiabatic process and every mutual host−guest configuration along the diffusion pathway can be characterized by its equilibrium relaxation properties. The center of mass of the guest molecule diffuses slowly inside the protein pore in comparison to the fast local intermolecular relaxation of the protein side chains and conformational relaxation of βCD itself. We utilize this natural separation of time scales to perform a set of all-atom equilibrium MD simulations for several starting positions of the guest molecule along the channel axis. One additional advantage of this hierarchical description of the overall βCD diffusion is that, in such formulation, the methodology is easily parallelizable for the distributed memory cluster-type computers, in which each processor generates an independent trajectory starting with unique initial conditions.[51]

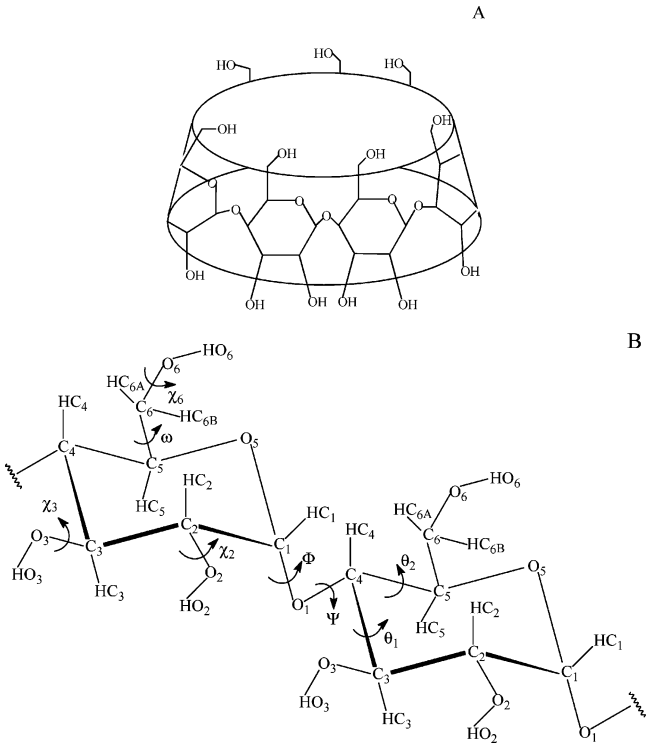

Figure 1. (A) Schematic representation of the structure of β-cyclodextrin (βCD) outlining its truncated cone shape. (B) Atomic labeling and geometry descriptors of βCD are based on refs 42, 52, and 57. Two glucose units of the 7-fold ring are shown. Glucose units are numbered from left to right. See details in the text.

The article is organized as follows. Section 1 is the introduction; in section 2, we describe the systems under investigation and the molecular dynamics methodology; in section 3, we present and discuss the results of the simulations in the context of the goals of the present study. These goals are to elucidate mechanisms of noncovalent protein−carbohydrate interactions, to characterize the diffusion of the flexible cyclic molecule in the confined environment of the protein channel and to predict the detailed structure of the αHL−βCD complex. In section 3.1, we report the dynamics of βCD in the channel on the nanosecond time scale and compare it with the dynamics of βCD in bulk water. In sections 3.2 and 3.3, energetics of αHL−βCD metastable complexes is assessed. In sections 3.4 and 3.5, MD results are compared with the experimental information from electrophysiological, mutagenesis, and thermodynamic studies. In sections 3.6 and 3.7, a thorough analysis of induced-fit effect that accompanies binding of βCD to the interior of the channel is presented, and the corresponding structural binding motif is described. Section 4 concludes the paper.

2. MD Simulation

2.1. The System Studied. β-Cyclodextrin is a cyclic oligomer composed of seven α-D-glucose units joined by α-(1,4) linkages.[13] βCD has a toroidal form and can be sketched as a truncated cone (Figure 1A). The narrower rim of the truncated cone contains seven primary hydroxyl groups, the wider rim contains 14 secondary hydroxyl groups. Both rims are hydrophilic, while the cavity is more hydrophobic due to hydrogen atoms and glycosidic oxygen bridges. The external diameter of the cone measures 15−16 Å, the diameter of the cavity varies from 5 to 8 Å, and the height of the molecule is ca. 8 Å.[13,52]

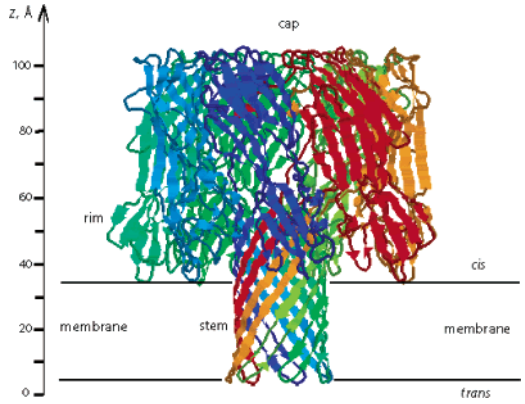

Figure 2. Ribbon representation of α-hemolysin (αHL) with a putative position of the lipid bilayer (membrane). Each chain of the protein is displayed in different color. Stem, rim and cap domains of αHL are marked. The cis and trans sides of the membrane are specified as well. The *z*-axis, defined as the symmetry axis of the channel, is shown displaced from the central position. Images were generated with RASMOL.[88]

α-Hemolysin is a protein toxin secreted from *Staphylococcus aureus* as a water-soluble 33.2 kDa monomer, which forms a mushroom-shaped membrane-inserted heptamer,[53] as shown in Figure 2. The channel-forming protein consists of seven chains, with 293 residues each. The structure of αHL has been resolved by X-ray diffraction at 1.9 Å resolution.[54] The stem domain, 52 Å in height and 26 Å in diameter, is formed as a 14-strand antiparallel β-barrel. The maximum diameter of the pore is 46 Å in the cap domain; the diameter of the pore in the stem domain varies from 14 (constriction region) to 24 Å. A schematic representation of the pore region is given in Figure 3A, with the location of several important amino acid residues indicated. The *z*-axis through the center of the pore, as it is used in further analysis, and a schematic representation of the βCD molecule in one possible orientation in the channel lumen are also shown in Figure 3. The constriction is formed by the side groups of Glu111, Lys147, and Met113 located at the top of the stem and projecting into the lumen of the β-barrel (Figure 3). The residues Asn139 and Leu135 represent wider constrictions in the lumen.

2.2. Initial Structures and Force Field Parameters. The structure of αHL protein was taken from Protein Data Bank (PDB), accession code 7AHL (resolution 1.9 Å).[54] Considering strong[23] experimental evidence that βCD blocks the channel for substantial periods of time only when added to the solution from the trans side of the channel (see Figure 2); it is a bottom of the channel molecule and that it never diffuses through the channel into the cis side of the membrane, only the transmembrane part of the channel and the region of the protein immediately adjacent to it have been included in the model. Thus, the partial model of the protein includes the entire β-barrel stem region, constituted by residues 108−152 of each chain (4592 atoms). The constriction in the channel, which presumably prevents the βCD from diffusing from the stem region into the much wider head region of the protein, was also included in our model. Water molecules were removed from the crystal structure and missing hydrogens were added with XLEAP program of the AMBER6 package.[55] The coordinates of the molecule were aligned along the principal axes, with the *z*-axis oriented along the 7-fold symmetry axis of the β-barrel toward

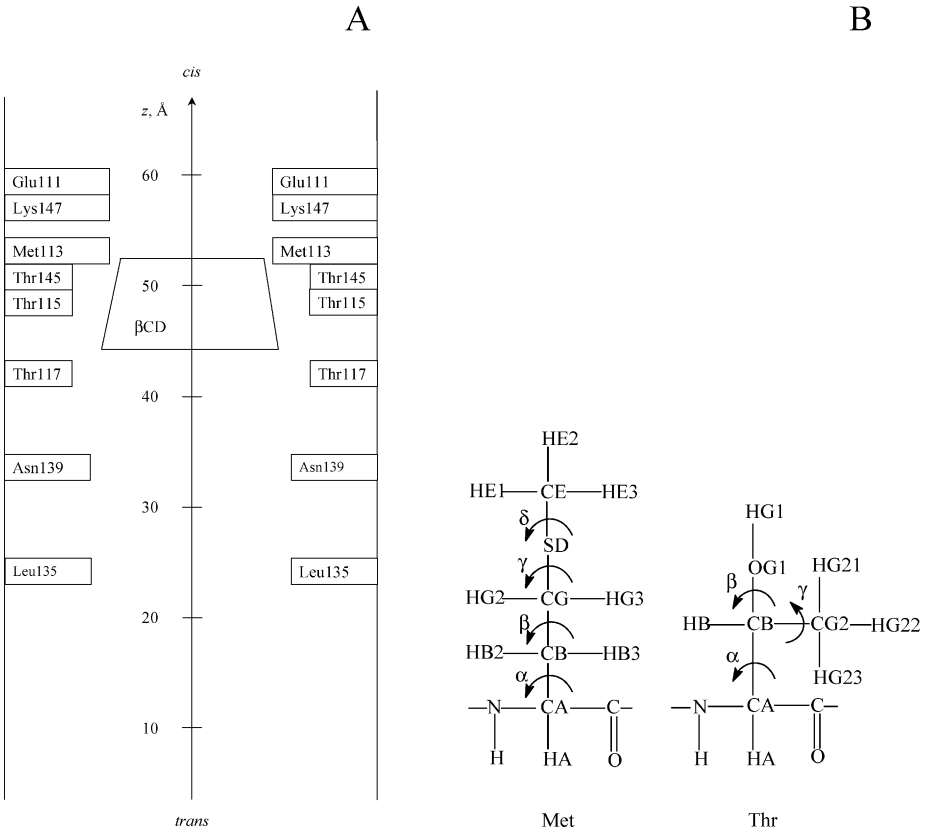

Figure 3. (A) Schematic diagram of the stem domain of αHL with βCD inside the pore. Residues Met113, Lys147, and Glu111 form constriction impenetrable for βCD. Residues Leu135 and Asn139 form wider constrictions. Other residues are not displayed. The *z*-axes scale is the same as in Figure 2 and as used in all the simulations and the analysis. (B) Schematic representation of amino acid residues Met and Thr with definition of dihedral angles. Angles of Met: α (HA−CA−CB−CG), β (CA−CB−CG−SD), γ (CB−CG−SD−CE), δ (CG−SD−CE−HE1). Angles of Thr: α (HA−CA−CB−CG2), β (CA−CB−OG1−HG1), γ (CA−CB−CG2−HG21).

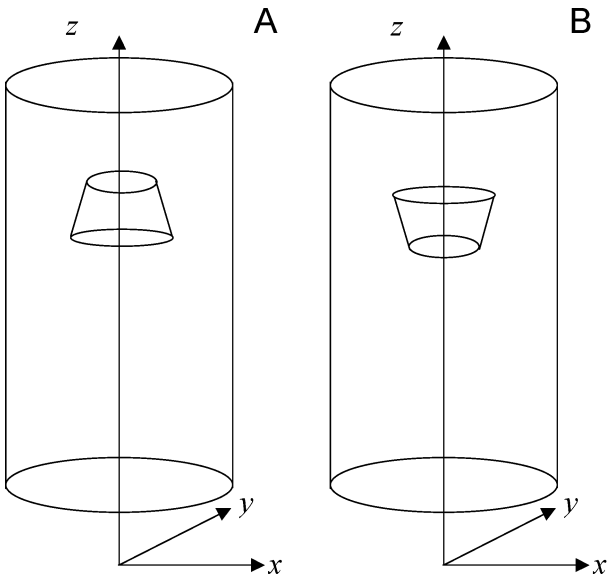

Figure 4. Schematic view of the models of αHL + βCD complex. See also Figure 3A for relative location of *z* axes. (A) Structures of A type. Structures A30, A35, A40, A45, and A50 are constructed by placing βCD at $z = 30$, 35, 40, 45, and 50 Å, with the narrower rim pointed upward. (B) Structures of B type. Structures B30, B35, B40, B45, and B50 are constructed by placing βCD at $z = 30$, 35, 40, 45, and 50 Å, with the narrower rim pointed downward.

the cap of αHL, from trans side to the cis side of the channel (Figures 2 and 3). The origin of the coordinate system was placed below the stem, so that the center of mass of β-barrel was at $z = 40$ Å, as shown in Figure 3. The height of the truncated structure used in further modeling was ca. 60 Å.

Coordinates of βCD were taken from the Protein Data Bank (PDB), accession code 1ACO.[16] The coordinates of the molecule were aligned along the principal axes. The *z*-axis of the molecule was directed from the wider toward the narrower rim (Figure 1A).

Cornell et al.[56] force field parameters were used in simulations for the protein. Partial atomic charges and the angle $O_5-C_1-O_1$ parameter for βCD (Figure 1B) were taken from the work.[57]

2.3. Model of the α-Hemolysin Ion Channel with β-Cyclodextrin in the Lumen of the Pore. The model of β-cyclodextrin bound to an α-hemolysin ion channel in a lipid bilayer and surrounded by water was constructed with XLEAP using the truncated αHL model as described in the previous section. Ten structures of αHL−βCD complex, with different positions and orientations of βCD with respect to the protein were prepared. In the first five structures further referred to as A30, A35, A40, A45, and A50, the narrower rim of βCD was oriented toward the cis side of the channel ("upward" orientation), and the center of mass of βCD was placed at $z = 30$, 35, 40, 45, and 50 Å, respectively. A schematic representation of a complex with the "upward" orientation is shown in Figure 4A. Five other structures were generated in a similar fashion but the narrower rim of βCD was oriented in the opposite direction ("downward" orientation), as shown in Figure 4B. The resulting structures are further referred to as B30, B35, B40, B45, and B50, according to the initial position of the ligand center of mass in the channel lumen. The starting points along the channel lumen were chosen to sample the internal part of the lumen available to the adapter upon entering the channel.

Each structure was installed in a slab of 1796 heavy (100 au) dummy atoms with Lennard-Jones parameters $\epsilon = 0.05$ kcal/mol and $R^* = 2.5$ Å, and no partial charge.[58] This nonpolar layer of dummy particles represents the interior of the lipid bilayer impermeable for water molecules, which is about 40 Å thick.[59] Also, it partially accounts for the rim domain of the protein itself. Each system was then solvated with TIP3P water[60] molecules, so that solvent molecules formed two slabs 10 Å in height above and below the membrane and filled the channel. The number of water molecules varied from 3018 to 3040 depending upon a specific system. To neutralize the total charge of the protein, 14 Na^+ counterions were placed on the outer surface of the β-barrel. The overall size of the system thus constructed was $73 \times 73 \times 88$ Å^3.

2.4. Molecular Dynamics Simulations. Energy minimization and molecular dynamics simulation were performed with the AMBER6 package. The energy of the system was minimized with 2000 steps of the steepest descents method followed by 1000 steps of the conjugate gradients method. During energy minimization positions of protein backbone atoms, all βCD atoms, Na^+ ions, and dummy atoms were restrained via the harmonic force with the constant 200 kcal/(mol·Å^2). Minimized structures were then equilibrated during 300 ps MD simulation at a constant pressure of 1 atm. Pressure regulation was performed using the Berendsen algorithm[61] with a coupling constant of 0.2 ps. The temperature was gradually increased from 0 to 300 K. The temperature of the system was maintained with the Berendsen algorithm[61] with a coupling constant of 1 ps. Positions of βCD and dummy atoms were kept fixed. Protein atoms were also frozen, with exception for the side chains of Glu111, Met113, Lys147, Asn139, and Leu135 to facilitate permeation of water molecules into the pore. Periodic boundary conditions were applied to the system. The particle-mesh Ewald (PME) method[62] was used for long-range electrostatic interactions. For van der Waals (vdw) nonbonded interactions, a 12 Å cutoff was applied. The bond lengths involving hydrogen atoms were constrained with the SHAKE algorithm,[63] allowing a 2 fs time step. Equilibration at constant pressure was followed by 50 ps of MD run at constant volume and constant temperature 300 K. Protein backbone atoms and glycosidic oxygens of βCD were restrained with the harmonic force constant 0.5 kcal/(mol·Å^2); dummy atoms and counterions were restrained with the force constant 200 kcal/(mol·Å^2).

In the course of the third, equilibrium, stage of MD simulation the restraints on the protein backbone, counterions, and dummy atoms remained the same, but all the atoms of βCD, protein side chains, and water were allowed to move.[90] The translational and rotational movement of the whole system was removed at the beginning of the simulation. An MD production simulation of 2 ns was performed for each system. Coordinates of all atoms were collected every 0.5 ps. Calculation of interaction energies between βCD and αHL and geometric analysis of trajectory files were performed using AMBER6. All calculations were carried out on dual AMD Athlon 1.2 GHz computers. It took 1 day to perform 70 ps of MD run of one system on a single CPU.

2.5. Simulation of β-Cyclodextrin in Aqueous Solution. An MD simulation of β-cyclodextrin in bulk water was also performed. One βCD molecule was solvated with 1175 TIP3P water molecules in the box with dimensions $34 \times 37 \times 30$ Å^3. The energy of the system was minimized by the steepest descents method for 2000 steps followed by 1000 steps of minimization by the conjugate gradients method. The system was heated from 0 to 300 K at constant pressure during 300 ps of MD simulation. The glycosidic oxygens of βCD were constrained with the harmonic force constant 0.5 kcal/(mol·Å^2). After the equilibration, 8 ns production MD trajectory of a free βCD with all constraints removed was generated at

constant volume and temperature $T = 300$ K. Other computational details were similar to those described above for the simulation of a channel model.

The diffusion coefficient was calculated using the linear regression of time dependence of the mean square displacement (MSD) of the center of mass of βCD according to the Einstein equation:[64]

$$\lim_{t\to\infty} \langle (\mathbf{r} - \mathbf{r}_0)^2 \rangle = 6Dt \quad (1)$$

where $\mathbf{r}$ is the position of the center of mass of a particle at time t and $\mathbf{r}_o$ is the position at time $t = 0$.

2.6. Energy Calculations. We first calculated the direct pairwise interaction energy E_{int} between αHL and the βCD molecule as a sum of van der Waals (vdw) E_{int}^{vdw} and electrostatic E_{int}^{ele} energies.[65] Second, the binding free energies (ΔG_{bind}) for αHL−βCD complexes were calculated on a continuum level as the sum of electrostatic ΔG_{elec} and nonpolar ΔG_{nonp} contributions:[66]

$$\Delta G_{bind} = \Delta G_{elec} + \Delta G_{nonp} \quad (2)$$

Electrostatic contribution to the binding free energy was calculated as the difference between electrostatic free energy of the complex surrounded by the membrane and water G_{elec} (αHL + βCD + membrane), αHL surrounded by the membrane and water G_{elec}(αHL + membrane), and βCD surrounded by water only G_{elec}(βCD):

$$\Delta G_{elec} = G_{elec}(\alpha\text{HL} + \beta\text{CD} + \text{membrane}) - G_{elec}(\alpha\text{HL} + \text{membrane}) - G_{elec}(\beta\text{CD}) \quad (3)$$

Electrostatic energy was calculated as $G_{elec} = (1/2)\sum_i q_i \varphi_i$, where q_i is a charge and φ_i is the electrostatic potential at the position of that charge.[67] The sum is taken over all partial charges in the system. Potential φ_i at the position $\mathbf{R}_i$ of the ith partial charge is obtained by numerically solving the Poisson equation

$$\nabla(\epsilon(\mathbf{R})\nabla\varphi(\mathbf{R})) = -4\pi\rho(\mathbf{R}) \quad (4)$$

where $\epsilon(\mathbf{R})$ is the dielectric constant and $\rho(\mathbf{R})$ is the density of fixed charges depending on position $\mathbf{R}$.

Equation 4 was solved numerically using the PNP program.[68] A three-dimensional dielectric constant map was generated using radii 1.7, 1.0, 1.5, 1.6, and 1.9 Å for C, H, N, O, and S, respectively, and the solvent probe radius 1.4 Å. Dielectric constant 4 was attributed to the membrane, protein, and βCD and 80 to bulk and channel water.[58] The Poisson equation was solved on a 301 × 301 × 301 grid with resolution of 3.2 grid points/Å. The atomic partial charges were the same as in the MD simulation.

The nonpolar contribution into the binding energy ΔG_{nonp} was estimated with the equation

$$\Delta G_{nonp} = \gamma[A(\alpha\text{HL} + \beta\text{CD}) - A(\alpha\text{HL}) - A(\beta\text{CD})] \quad (5)$$

where A(αHL + βCD), A(αHL), and A(βCD) are the solvent-accessible surface areas[69] of the complex, αHL, and βCD, respectively. The solvent-accessible surface area was calculated with the SASA program.[70] The parameter γ was set to 7.2 cal/(mol·Å^2).[71]

3. Results and Discussion

3.1. Dynamics of β-Cyclodextrin Inside the Channel. Starting with 10 initial positions of cyclodextrin, approximately evenly distributed along the αHL channel axis, as described in section 2.3, the βCD molecule was allowed to move freely inside the pore lumen in the course of ca. 2 ns MD simulation. The goal of this "experiment" was to probe the dynamic behavior of βCD inside the channel lumen. If several binding sites for βCD exist in the channel, the time scale of the overall diffusion of βCD inside the pore can be long, inaccessible by a direct simulation. The distribution of starting configurations along the channel axis allowed us to investigate host−guest interactions and possible binding sites, even though the total time of the simulation is shorter than the characteristic time required for the guest molecule to enter and leave the channel. Figure 5 summarizes the time evolution of z-coordinate of βCD center of mass for all simulated systems. This coordinate characterizes the diffusion of βCD as a whole. As seen in Figure 5 the maximum deviation from the initial z-coordinate did not exceed 6 Å in all systems, i.e., βCD exhibited a trend to bind at certain positions in the pore on the time scale of the simulation. In the systems A45, A50, B45, and B50 βCD was trapped in position with $z \approx 48$ Å; similarly, evolution of systems A35 and A40 resulted in location of βCD near $z = 37-38$Å, and the systems B30 and B35 converged to the state with $z = 31-32$Å. The rotation of βCD has been hindered. These observations indicate the existence of at least three possible binding sites. In contrast, the results of the simulation of the free βCD in bulk water on the similar time scale (8 ns of total simulated time) clearly demonstrated uninhibited translational and rotational mobility. The calculated diffusion coefficient of βCD in bulk water $D = (4.4 \pm 0.2) \times 10^{-6}$ cm^2/s is in good agreement with the experimental value $D = 3.21 \times 10^{-6}$ cm^2/s.[72] The simulation of βCD in bulk water provides a characteristic time scale for the mobility and the conformational flexibility of the free βCD. It also serves as a tool to validate the potential functions and other parameters used in the simulations.

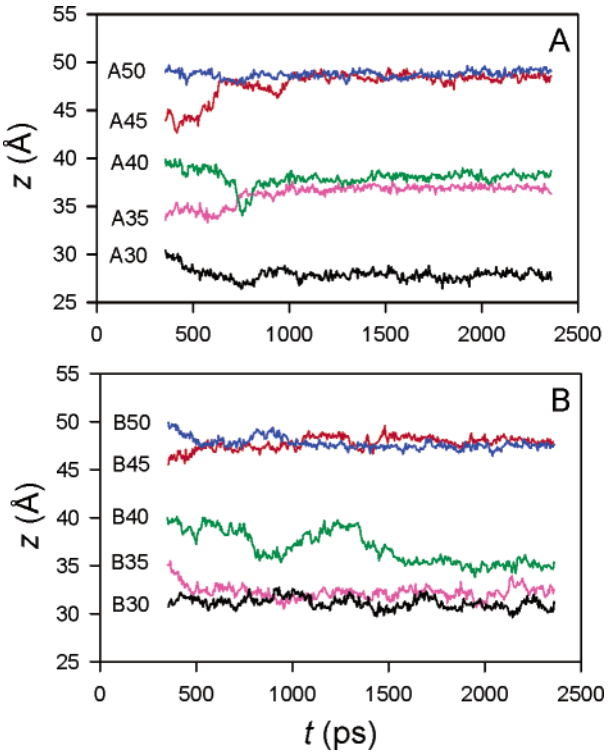

Figure 5. Time evolution of z-coordinate of the center of mass of βCD: (A) structures A30−A50; (B) structures B30−B50. The structures are named according to the initial position and are marked in the figure.

TABLE 1: Geometric Parameters of β-Cyclodextrin Averaged over the Time Period from 1300 to 2300 ps: *z*-Coordinate of the Center of Mass, Angle φ Between the Molecular *z*-Axis and the *z*-Axis of the System, Distance *r* between the Center of Mass and the Channel *z*-Axis, Where the Mean Value ± Standard Deviation (SD) Is Given for Each Observable

system	$\langle z \rangle$ (Å)	$\langle \varphi \rangle$ (deg)	$\langle r \rangle$ (Å)	system	$\langle z \rangle$ (Å)	$\langle \varphi \rangle$ (deg)	$\langle r \rangle$ (Å)
A30	27.8 ± 0.4	16 ± 8	0.8 ± 0.4	B30	30.9 ± 0.5	159 ± 8	1.9 ± 0.2
A35	36.9 ± 0.3	72 ± 5	4.7 ± 0.2	B35	32.1 ± 0.6	144 ± 15	2.0 ± 0.5
A40	38.1 ± 0.3	59 ± 5	4.4 ± 0.2	B40	35.7 ± 1.2	148 ± 8	2.5 ± 0.3
A45	48.4 ± 0.4	10 ± 5	0.3 ± 0.2	B45	48.0 ± 0.4	165 ± 9	0.9 ± 0.4
A50	48.8 ± 0.4	12 ± 6	0.4 ± 0.2	B50	47.4 ± 0.3	173 ± 4	0.3 ± 0.2

TABLE 2: Energy of Interaction E_{int} between β-Cyclodextrin and α-Hemolysin Averaged over the Time Period from 1300 to 2300 ps, and Its van der Waals E_{int}^{vdw} and Electrostatic E_{int}^{ele} Contributions, Mean Value ± SD, kcal/mol

system	E_{int}	E_{int}^{vdw}	E_{int}^{ele}	system	E_{int}	E_{int}^{vdw}	E_{int}^{ele}
A30	−71 ± 6	−60 ± 4	−11 ± 6	B30	−61 ± 5	−46 ± 2	−15 ± 5
A35	−78 ± 6	−60 ± 3	−18 ± 5	B35	−58 ± 7	−46 ± 3	−12 ± 6
A40	−80 ± 6	−57 ± 3	−23 ± 6	B40	−63 ± 7	−48 ± 3	−15 ± 6
A45	−84 ± 6	−64 ± 3	−20 ± 5	B45	−68 ± 7	−57 ± 3	−11 ± 6
A50	−86 ± 6	−64 ± 4	−22 ± 6	B50	−75 ± 7	−60 ± 3	−15 ± 7

To fully characterize the motion of βCD in the pore environment, we also calculated its tilt with respect to the channel axis and the deviation from the coaxial position. The tilt is represented by the angle φ between the molecular *z*-axis of βCD and the *z*-axis of the channel, and the off-center displacement is characterized by the distance *r* between the center of mass of βCD and the *z*-axis of the channel. For all studied systems the rotation of βCD was hindered, and only librational motion was observed. All geometric parameters relaxed to equilibrated values after approximately 1 ns, and configurations of the systems over the last 1 ns of simulation were used in further analysis.

The geometric parameters characterizing relative position of βCD in the channel are listed in Table 1. The final states of βCD within the channel can be roughly subdivided into three types: (1) βCD preserves the approximately symmetric alignment relative to the *z*-axis of the channel with the tilt angle $\langle \varphi \rangle < 25°$ or $(180 - \langle \varphi \rangle) < 25°$ and the off-center displacement $\langle r \rangle < 3$ Å (systems A30, A45, A50, B30, B45, and B50) as shown in Figure 6A; (2) βCD is tilted with the angle $\langle \varphi \rangle > 25°$ or $(180 - \langle \varphi \rangle) > 25°$, but its center of mass does not deviate far from the symmetry axis of the channel $\langle r \rangle < 3$ Å (systems B35 and B40), see Figure 6B; (3) βCD is bound to the wall of the channel with $\langle \varphi \rangle > 40°$ or $(180 - \langle \varphi \rangle) > 40°$ and $\langle r \rangle > 4$ Å (systems A35 and A40), as in Figure 6C.

3.2. Interaction Energy. One can conclude from the results shown in Figure 5 that there are several residence sites for βCD inside the αHL pore lumen. On the time scale of the MD simulation, however, it is impossible to estimate how long the βCD molecule can reside at one of these observed bound positions. It appears that the diffusion of the βCD molecule inside the αHL pore lumen proceeds through the chain of possible intermediate states on the time scale longer than several nanoseconds. Comparison of the relative binding energy, or the relative strength of protein−βCD interactions, for different configurations of the complex allows us to judge which of the observed binding sites is the most stable one. The most stable configuration can indicate a possible unique binding site of βCD inside the protein lumen, as predicted by experimental observations.[23]

Table 2 presents average values of calculated interaction energy (see section 2.6) for all systems along with its electrostatic and nonpolar contributions. The most negative values are obtained for the systems A45 and A50, i.e., when βCD is located just below the constriction formed by the Met113 side groups, as in Figure 6A. The most negative interaction energies among systems B, with downward orientation of βCD, are also observed for B45 and B50. Note also, that interaction energies calculated for all systems type B are higher than interaction energies of corresponding systems A. This result supports the suggestion that the "upward" orientation of βCD is more favorable than the "downward" one. For all systems the nonpolar contribution to the interaction energy dominates over the electrostatic one.

In Table 3, the contributions to the interaction energies from several amino acid residues are reported. The most important amino acid residues of αHL, i.e., the residues that give rise to 79−85% of the total interaction energy between βCD and αHL in the systems A45, A50, B45, and B50 are Glu111, Met113, Thr115, Thr145, and Lys147 (see Figure 3 for the relative location of these residues along the channel pore). Note, that the adaptor orientation is nearly coaxial with the channel axis at the binding site near the constriction formed by Met113 (this binding position resulted from the simulations of the systems A45, A50, B45, and B50). Interaction of βCD with uncharged residues Met113, Thr115, and Thr145 is attractive with the dominant vdw term. In systems A45, A50 interaction is repulsive with negatively charged Glu111 and attractive with positively charged Lys147. Interactions with both groups are governed largely by electrostatic effects. This observation suggests that the residence time of βCD in the channel lumen can be sensitive to mutations of any of these five amino acids, not only Met113 as was found in the experiment.[25] One can also predict that mutation of Glu111 to a positively charged residue would increase binding affinity to βCD. Similarly, mutation of Lys147 to a residue with a negative charge is expected to decrease the residence times of βCD. Such experiment could test our conclusions and also further corroborate the original idea of the residence position of βCD in the αHL channel. The decomposition of interaction energy into contributions from specific residues shows that the energetic preference of the systems A over systems B cannot be attributed to the interaction with a single residue; rather, several groups are responsible for this difference.

It is important to note that interaction energy does not provide the correct estimate of the binding free energy for the complex because it neglects entropy penalties, conformational rearrangements of participating molecules, and solvation contributions. In the next subsection, we will estimate the αHL−βCD binding free energies by a continuum methodology, in which the influence of the environment polarizability is taken into account using the mean-field approximation.

3.3. Binding Free Energy. In this section, we report calculation of the αHL−βCD binding energy using the con-

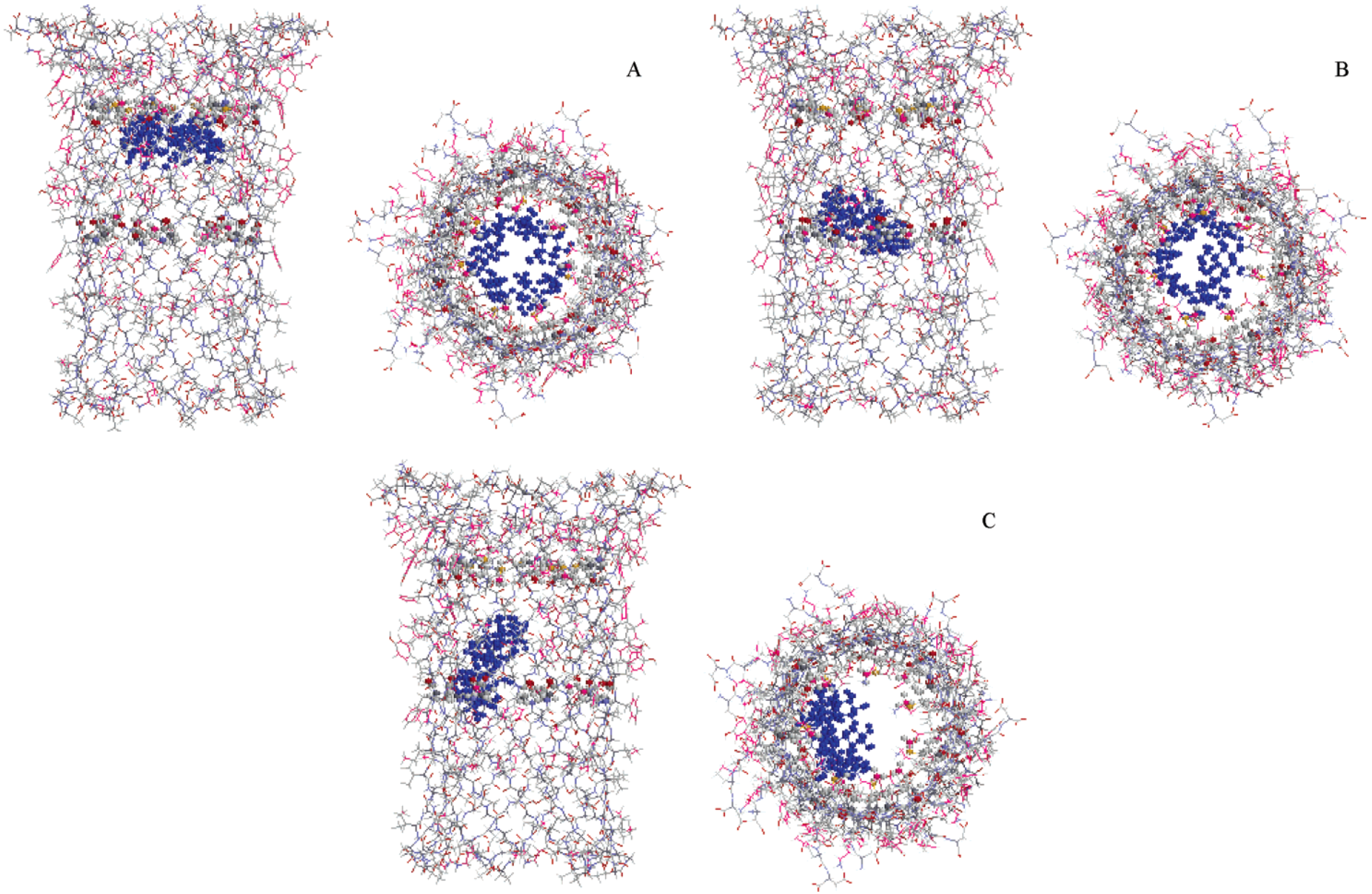

Figure 6. Final configurations of the system A45 (A), B40 (B), and A40 (C). The protein is represented as all-atom wireframe. The upper ring of residues displayed as ball-and-stick are Met113, the lower ring of residues are Asn139. βCD (blue) is shown as ball-and-stick. Water molecules and dummy atoms are not displayed.

TABLE 3: Interaction Energy of βCD E_{int} with Some Residues of αHL for the Systems A45, A50, B45, and B50, Averaged over the Time Period from 1300 to 2300 ps, with the van der Waals E_{int}^{vdw} and Electrostatic E_{int}^{ele} Contributions, Mean Value ± SD, kcal/mol

A45				A50			
group	E_{int}	E_{int}^{vdw}	E_{int}^{ele}	group	E_{int}	E_{int}^{vdw}	E_{int}^{ele}
Glu111	7.2 ± 4.7	−0.6 ± 0.1	7.8 ± 4.7	Glu111	8.0 ± 4.7	−0.8 ± 0.1	8.8 ± 4.7
Met113	−20.3 ± 2.5	−18.4 ± 1.8	−1.9 ± 1.8	Met113	−22.1 ± 3.1	−19.5 ± 2.1	−2.6 ± 1.8
Thr115	−20.9 ± 2.9	−16.1 ± 1.8	−4.8 ± 2.6	Thr115	−18.5 ± 3.1	−14.7 ± 1.7	−3.8 ± 3.2
Thr145	−17.6 ± 2.6	−14.8 ± 1.8	−2.8 ± 2.1	Thr145	−20.7 ± 3.1	−16.3 ± 1.6	−4.4 ± 3.0
Lys147	−18.6 ± 7.6	−1.9 ± 0.4	−16.7 ± 7.5	Lys147	−19.9 ± 7.8	−2.5 ± 0.5	−17.4 ± 7.7
total	−70.2 ± 6.2	−51.8 ± 3.1	−18.4 ± 5.1	total	−73.2 ± 6.3	−53.8 ± 3.6	−19.4 ± 5.5
B45				B50			
group	E_{int}	E_{int}^{vdw}	E_{int}^{ele}	group	E_{int}	E_{int}^{vdw}	E_{int}^{ele}
Glu111	−0.9 ± 4.7	−0.5 ± 0.1	−0.4 ± 4.7	Glu111	−0.4 ± 4.1	−0.4 ± 0.1	0.0 ± 4.1
Met113	−16.4 ± 2.8	−14.7 ± 2.0	−1.7 ± 1.7	Met113	−15.1 ± 2.6	−13.1 ± 1.8	−2.0 ± 1.7
Thr115	−17.2 ± 2.9	−14.7 ± 1.7	−2.5 ± 2.5	Thr115	−22.1 ± 3.3	−18.2 ± 1.7	−3.9 ± 2.8
Thr145	−17.1 ± 3.9	−12.2 ± 1.7	−4.9 ± 3.6	Thr145	−19.2 ± 3.6	−13.1 ± 1.3	−6.1 ± 3.9
Lys147	−2.4 ± 7.2	−1.6 ± 0.5	−0.8 ± 7.3	Lys147	−3.5 ± 6.8	−1.3 ± 0.3	−2.2 ± 6.8
total	−54.0 ± 7.7	−43.7 ± 3.7	−10.3 ± 6.6	total	−60.3 ± 6.9	−46.1 ± 2.8	−14.2 ± 6.2

TABLE 4: Binding Free Energy ΔG_{bind} for βCD and αHL with the Electrostatic ΔG_{elec} and Nonpolar ΔG_{nonp} Contributions Averaged over the Time Period from 1300 to 2300 ps, Mean Value ± SD, kcal/mol

system	ΔG_{bind}	ΔG_{elec}	ΔG_{nonp}	system	ΔG_{bind}	ΔG_{elec}	ΔG_{nonp}
A30	4.7 ± 1.4	13.1 ± 1.5	−8.4 ± 0.2	B30	3.4 ± 1.3	9.9 ± 1.5	−6.5 ± 0.4
A35	4.4 ± 1.1	11.6 ± 1.1	−7.2 ± 0.2	B35	2.6 ± 1.0	9.3 ± 1.2	−6.7 ± 0.4
A40	2.2 ± 1.1	9.1 ± 1.1	−6.9 ± 0.2	B40	3.3 ± 1.4	10.0 ± 1.6	−6.7 ± 0.3
A45	0.5 ± 0.9	9.8 ± 1.1	−9.3 ± 0.4	B45	2.1 ± 1.2	10.7 ± 1.2	−8.6 ± 0.3
A50	0.9 ± 1.0	9.8 ± 1.2	−8.9 ± 0.3	B50	1.2 ± 1.4	10.0 ± 1.4	−8.8 ± 0.2

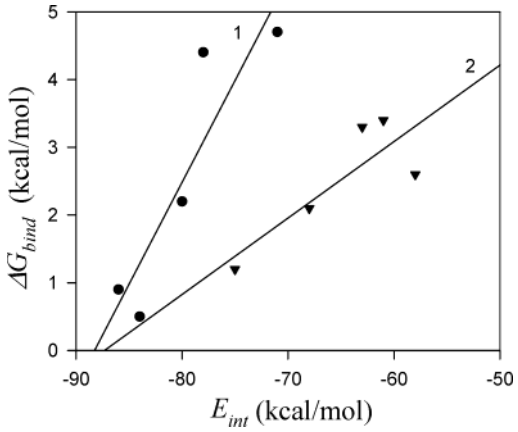

Figure 7. Correlation between the calculated interaction energy E_{int} and the binding energy ΔG_{bind} for the systems A30−A50 (circles) and B30−B50 (triangles). Lines 1 and 2 represent linear regression lines for the systems A30−A50 and B30−B50, respectively. Correlation coefficient for linear regression is 0.82 for the first group of systems and 0.69 for the second one.

tinuum representation of the surrounding water and the lipid bilayer as described in section 2.6.

The average values of the binding free energy presented in Table 4 for all the systems studied correlate well with the average interaction energies presented in Table 2. For example, the systems A45 and A50 both exhibit the lowest interaction energies and binding free energies. The correlation between the averaged interaction energy E_{int} and the binding energy ΔG_{bind} becomes more clearly pronounced if analyzed separately for the systems A30−A50 and B30−B50, as shown in Figure 7.

The binding free energy ΔG_{bind} calculated by eq 2 accounts for electrostatic interactions between molecules and all solvation effects, both electrostatic and nonelectrostatic. It does not, however, include entropic penalties upon binding, nor vdw interactions between αHL and βCD. The free energy change due to conformational rearrangements of molecules is not included in eq 2 either, although the flexibility of the protein and the ligand was taken into account by averaging binding energies for the "preconfigured" molecules along the trajectory as described in.[58] The energetic significance of subtler structural features, such as hydrogen bonding, is also beyond the grasp of the present analysis. Additional source of uncertainty comes from the choice of parameters of the model, such as dielectric constant of the protein or the membrane. Although a more elaborate combination of molecular mechanics (MM) force field and continuum electrostatics together with MD simulation was proposed[73] and even more detailed free energy decomposition methods were realized for single sets of X-ray structures[74,75] with variable success in predicting absolute binding free energies, we believe that the use of more intricate computational schemes is inexpedient for our systems due to artificial constraints and truncated protein structure utilized in this simulation.

3.4. Comparison with Electrophysiological Experiments Combined with Site-Directed Mutagenesis Studies. Interaction between βCD and αHL has been studied experimentally by recording ionic currents through a single channel formed by αHL in an artificial lipid bilayer.[21] Partial reversible current blockades were observed when βCD was added from the trans side of the membrane, but no current blocks occurred when βCD was added from the cis side. When bound within the lumen of the αHL pore βCD reduced conductance of the channel to 33−43% of the initial value. There was only one level of current blockade detected in each experiment. This observation allowed[21,23] the suggestion that there is only one binding site for βCD within the channel. The results of site-directed mutagenesis gave some additional evidence on the location of the predicted binding site.[23,25] It was shown that the residence time was prolonged up to tens of seconds when Met113 was substituted by Val, His, Tyr, Asp, Asn, or Phe. Mutations at some other positions of αHL, e.g. L135N, did not affect the affinity to βCD. These results suggested that βCD binds in the vicinity of Met113

but the particular role of this residue in binding βCD remained unclear.

Our results show that the configurations of the system with βCD near Met113 are, indeed, characterized by the most negative interaction and binding energies and preserve symmetric alignment within the channel during 2 ns. Thus, the results of our MD simulation confirm the earlier proposed location of the binding site. However, the contributions to the interaction energy from the residues close to Met113, i.e., Glu111, Thr115, Thr145, and Lys147, are equally important; therefore, mutations of these residues are expected to alter binding affinity. According to the results of the MD simulation there is more than one binding site for βCD in the wild-type αHL. The presence of such metastable states is not surprising because the interaction between αHL and βCD lacks specificity. The presence of alternative binding sites will certainly affect dynamics and diffusion of βCD in the channel pore.

Our simulated model predicted that the upward orientation of βCD, with narrower rim pointing to the cis side of the membrane, is more favorable than the downward orientation. Experimental results did not distinguish between the two orientations of βCD in the binding site. Both orientations allow host−guest complexation with small organic molecules within the channel, as was observed experimentally.[23,24] Hence, additional experimental evidence may be necessary to confirm or refute this computational result. Such experiment might use a guest molecule that binds preferably from the wider rim of βCD.

3.5. Comparison with Thermodynamic Studies of Protein−Carbohydrate Interactions. Protein−carbohydrate interactions are usually characterized by weak affinities with free energy changes in the range −4 to −8 kcal/mol.[1,2,4] The entropies of binding are negative in the most cases; therefore, protein−carbohydrate interactions can be considered to be enthalpy-driven. Thermodynamic data show a clear-cut enthalpy−entropy compensation effect. The relative significance and sometimes even the sign of the effects of hydrogen bonding, solvation, hydrophobic interactions, and ligand and protein flexibility on thermodynamics of protein−carbohydrate binding are still in dispute.[1,11,12] The binding affinity of βCD to αHL calculated from the association constant reported in ref 21 is 2-fold smaller ($\Delta G^\circ = -3$ kcal/mol at pH 7.5 and 295 K) than that found for glucoamylase[76] and maltodextrin binding protein (MBP),[77] indicating the lack of specificity of αHL for carbohydrates. Some mutated αHLs, e.g., mutant M113N, exhibited larger affinity of up to $\Delta G^\circ = -9$ kcal/mol,[25] exceeding those of glucoamylase and MBP.

Attempts to predict the binding specificity of proteins to different carbohydrate ligands using MD simulation have recently been reported. Methods of thermodynamic integration (TI)[31] or free-energy perturbation (FEP)[34,36,37] have been used. One of the recent works[36] has shown that the FEP simulation cannot always reproduce relative binding affinities with the accuracy of 0.5−1.0 kcal/mol. The uncertainties in calculated relative free energies were commensurable with the values themselves. Although the authors paid considerable attention to the force field parameters and protonation states of the protein side groups, only qualitative agreement with experiment was achieved for some ligands. Applications of MM/PBSA method[73] to estimate the RNA−protein and protein−ligand absolute binding affinities without explicitly adjustable parameters were shown, in some cases, to give errors up to 10 kcal/mol.[78,79] Similar discrepancies with experiment are expected for the binding of ligands to the membrane proteins. However, application of semiempirical approaches such as linear interaction energy (LIE) approximation to predict absolute binding free energy for protein−carbohydrate complexes was shown to be promising,[33] and better agreement can be expected with more extensive parametrization.[80]

We did not make an attempt to calculate the absolute binding free energy for the αHL−βCD complex due to the difficulties mentioned above. In the present study, we use both interaction energy E_{int} and binding energy ΔG_{bind} to characterize the relative stability of the αHL−βCD complexes for different positions and orientations of βCD in the lumen of the pore. Our results demonstrate (see sections 3.2 and 3.3) that, although not free from uncertainties, both methods supplement each other in describing the influence of different parts of confined environment of αHL and particular residues on the stability of the complex.

Decomposition of the interaction energy reveals the predominance of vdw interactions over electrostatics (see Table 2). Hence, it is not surprising that electrostatic contribution into the binding energy was found to be unfavorable (Table 4). The nonpolar contribution to the binding energy favors association, reflecting a well-known, but still poorly understood, hydrophobic effect.[81] The fact that both the interaction E_{int} and binding energy ΔG_{bind} point to the most stable location of βCD, in agreement with experiment, and show close correlation between each other is encouraging.

3.6. Conformational Analysis. The induced-fit effect upon the αHL−βCD association, i.e., mutual conformational rearrangement of both molecules involved in interaction, is analyzed in this section. First, we compare the conformational flexibility of βCD molecule inside the channel pore and in water solution. Conformational flexibility of βCD is characterized here by a number of geometric descriptors shown in Figure 1B and described below. The glucosidic torsion angles are defined as Φ (HC1−C1−O1−C4*) and Ψ (HC4−C4−O1*−C1*), following ref 42. The orientation of O6 atom relative to the pyranose ring is described by the angle ω (HC5−C5−C6−O6). Rotations of hydroxyl groups O2−HO2, O3−HO3, and O6−HO6 are described by the torsion angles χ_2 (HC2−C2−O2−HO2), χ_3 (HC3−C3−O3−HO3), and χ_6 (C5−C6−O6−HO6), respectively. The conformations of glucose units are characterized by endocyclic torsion angles θ_1 (C2−C3−C4−C5) and θ_2 (C3−C4−C5−O5). The overall shape of the macroring is characterized by O1 (i) − O1 ($i \pm 3$) distances, where i denotes the number of a glucose unit.

The distribution of dihedral angles for the βCD in the bulk water is shown in Figure 8A in the vein of Ramachandran plots.[66] The distribution of angles for βCD confined within the channel is shown in Figure 8A. Comparing corresponding panels in Figure 8, one can see that most conformational descriptors of βCD molecule remain unchanged upon entering the channel. The significant difference in conformational behavior between the "free" and "confined" states of βCD is displayed by distributions of the Ψ angle, which characterizes the tilt of one glucose ring in and out the βCD cavity (Figure 8A,B, panels 1). In aqueous solution, the Ψ angle frequently adopts *trans*-conformation ($120^\circ < \Psi < 180^\circ$), which corresponds to the glucose ring tilted toward the cavity of βCD. Such conformations are completely inhibited in the channel due to the repulsion from the walls of the pore. The quantitative analysis of the distribution of the torsion angles reveals that interaction with the walls of the channel favors trans conformations of the dihedral angle ω (compare panels 3 in Figure 8A,B), with the O6 atom pointing outward from the βCD cavity. The fraction of trans conformations, i.e., $120^\circ \le \omega \le 180^\circ$ and $-180^\circ \le \omega$

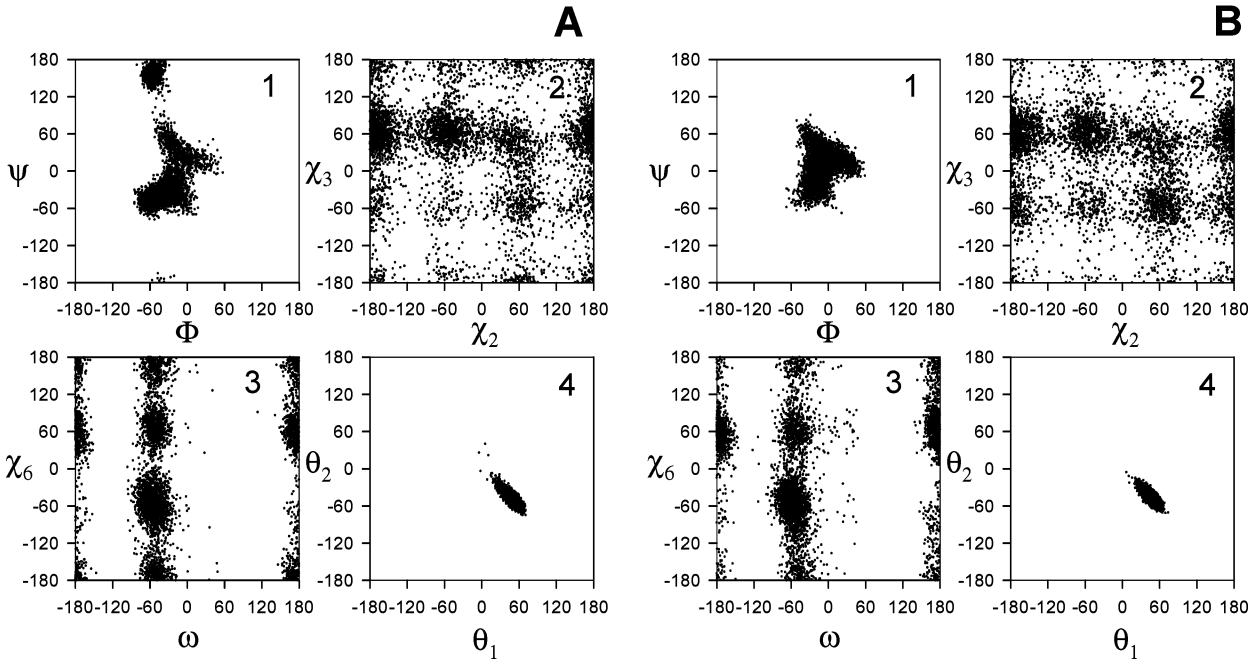

Figure 8. (A) Distribution of torsion angles (degrees) describing conformational movement of βCD in bulk water. Each dot corresponds to a pair of angles in one glucose unit in one snapshot. Key: (1) Φ (HC1−C1−O1−C4*), Ψ (HC4−C4−O1*−C1*); (2) χ_2 (HC2−C2−O2−HO2), χ_3 (HC3−C3−O3−HO3); (3) ω (HC5−C5−C6−O6), χ_6 (C5−C6−O6−HO6); (4) θ_1 (C2−C3−C4−C5); θ_2 (C3−C4−C5−O5) See Figure 1B for the atomic labels. (B) Same as part A for βCD confined inside the protein barrel (the simulated system A45).

$\leq -120°$, is 16% in bulk solvent, whereas for the systems A30−A50 it varies between 21 and 45%. No substantial difference in distribution of the angles χ_2, χ_3, χ_6, θ_1, and θ_2, describing rotation of hydroxyl groups and endocyclic conformations of pyranose rings, was observed for the free and confined states of βCD (Figure 8).

The average "diameter" of the macroring, i.e., O1 (i) − O1 ($i \pm 3$) distance, is 9.7 ± 0.2 Å for βCD both in bulk water and in the channel. The average conformation of the βCD macroring, therefore, remains the same, as the molecule enters the channel lumen. However, the average range of diameters, i.e., the difference between the maximum and minimum values in the same molecule, differs for the free and bound βCD. The macroring diameter range is a measure of how far the ring deviates from the circular shape. It equals 3.1 ± 0.7 Å for the βCD in bulk water and 1.4 ± 0.6 Å when βCD is in the channel. This observation indicates that the macroring maintains the same diameter in bulk water and in the channel, but it is considerably more flexible in the bulk.

The reduction of conformational flexibility of oligosaccharides upon binding to a protein was also analyzed in other computational works.[32,35] In our study, the change of conformational flexibility of βCD should be attributed not merely to interactions with amino acid residues on the protein surface, but to the more global effect of the confined environment of the pore.

The effect of βCD on conformational motion of the protein side groups projected into the lumen is characterized by distributions of dihedral angles of Met113, Thr115, and Thr145 residues: Definitions of corresponding angles are given in Figure 3B. We have compared the dynamics of these residues in the systems A30 and A50 to investigate how the close proximity of the guest molecule influences the behavior of the protein side chains. For example, A50 is one configuration when βCD was bound in a close contact with Met113 during the simulation. In the system A30, βCD is located relatively far from the Met113; therefore, we can assume that the behavior of this side-chain was unaffected by the presence of βCD. The most favored conformation for the β angle is the trans conformation, but the free Met113 also exhibits a slightly populated conformation with β around −80°, which was not observed in the systems A45, A50, B45, and B50. Other torsion angles of Met113 remain unaltered upon binding of βCD. In residues Thr115 and Thr145 only the angle β, which characterizes the rotation of the hydroxyl group, shows considerable dependence on proximity of βCD (see Figure 9). We found that in the absence of βCD the conformations of β around −80° and +80° are evenly populated, whereas the presence of βCD in the vicinity of these residues favors only one of these conformations (Figure 9). Nevertheless, this effect is much less pronounced in the system A50 compared to A45, B45, and B50.

3.7. Hydrogen Bonding. Hydrogen bonding has long been considered essential for the structure of both cyclodextrins[42,44,83] and the protein−carbohydrate interface.[2,3,84] Several examples of crystal and solution structures of protein−βCD complexes have been reported recently, namely complexes with *Aspergillus niger* glucoamylase,[16] soybean β-amylase,[17] maltodextrin binding protein (MBP),[18] and *Thermoactinomyces vulgaris* R-47 α-amylase 2.[19,20] Most of these studies were aimed at understanding catalytic activity of starch-degrading enzymes, and βCD was selected as a model ligand, a cyclic analogue of starch. In the work,[18] a MBP−βCD complex was studied in order to compare its structure with those of other complexes involving oligosaccharides of physiological importance. Though protein−carbohydrate interactions on the whole reveal a diversity of structural motifs,[2] the structures of the four different protein−βCD interfaces[16−18] show considerable similarity. The main features of these interactions are: a remarkably small number of direct hydrogen bonds (1, 4), several (4, 5) water-mediated hydrogen bonds, and stacking interactions between glucose units and aromatic side chains of the residues Phe, Tyr, and Trp. The structure obtained in ref 19 is less informative due to poorer resolution (3 Å) but is still consistent with this binding motif. It should be noted, however, that the binding mode in solution

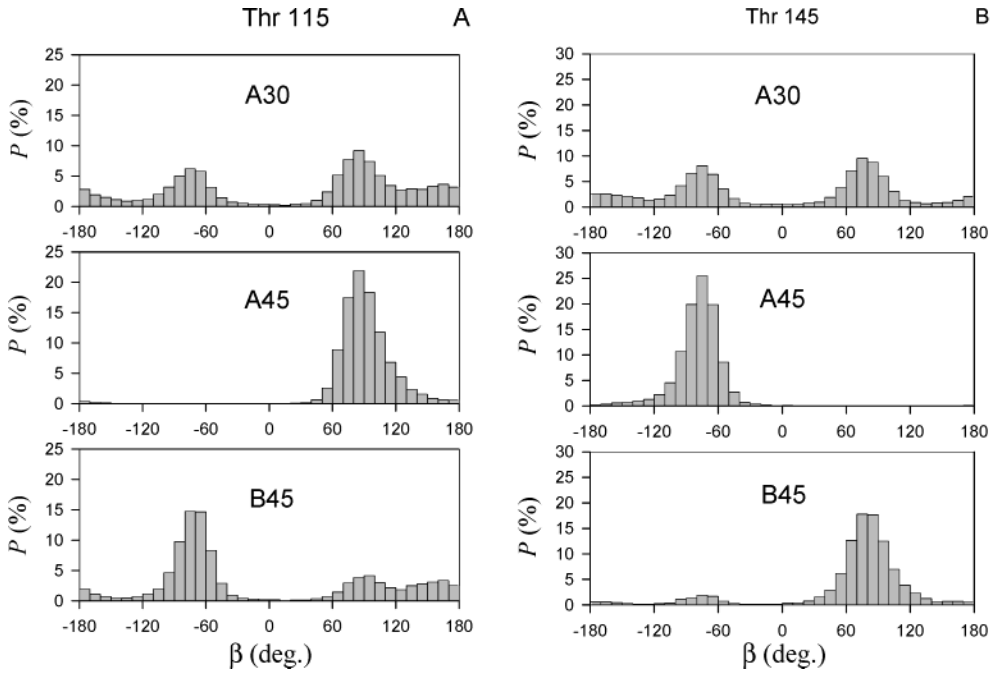

Figure 9. (A) Probability distribution (P) of the torsion angle β of Thr115 describing the conformation rearrangement of the protein upon binding of βCD. βCD is far from Thr115 in the system A30 and in close contact with this residue in A45 and B45. See Figure 3B for the atomic labels. (B). The same for Thr145 in the system A30 and in close contact of βCD with this residue in A45 and B45.

TABLE 5: Average Occupancies of Intermolecular Hydrogen Bonds in βCD, %

hydrogen bond type	A30	A35	A40	A45	A50	bulk water
O2−HO2 (i)···O1 (i)	22	19	19	20	21	25
O2−HO2 (i)···O3 (i)	14	12	13	13	15	11
O2−HO2 (i)···O3 ($i+1$)	39	21	20	32	33	12
O3−HO3 (i)···O1 ($i-1$)	12	14	15	15	17	7
O3−HO3 (i)···O2 (i)	40	35	34	37	34	42
O3−HO3 (i)···O2 ($i-1$)	21	17	15	23	26	8
O6−HO6 (i)···O5 (i)	26	30	22	37	40	29

TABLE 6: Average Composite Occupancies of Hydrogen Bonds between βCD and Water, %

hydrogen bond type	A30	A35	A40	A45	A50	bulk water
O2−HO2···OH_2	47	87	77	76	75	101
HO−H···O2	60	123	118	107	111	139
O3−HO3···OH_2	58	88	86	78	72	98
HO−H···O3	53	109	110	100	98	120
O6−HO6 ···OH_2	86	49	59	44	40	88
HO−H···O6	128	73	101	101	102	136
HO−H···O1	20	20	23	21	21	28
HO−H···O5	60	40	37	18	12	63

can be different from that in the crystal. For example, the binding cleft of the MBP protein in solution is 11° more closed than in the X-ray-derived structure, as shown by recent NMR studies.[85]

We consider three types of hydrogen bonds: (1) intramolecular hydrogen bonds of βCD, (2) hydrogen bonds between βCD and water, and (3) hydrogen bonds between βCD and Thr115, Thr145 (in the systems A45, A50, B45, and B50). We assume that a hydrogen bond O(1)−H(1)···O(2) is formed when the following geometric conditions are satisfied: the distance O(1)−O(2) ≤ 3.5 Å and the angle H(1)−O(1)−O(2) ≤ 60°. The occupancies of the most frequently observed intramolecular βCD hydrogen bonds are listed in Table 5. The occupancies of the hydrogen bonds within the same glucose subunit are similar for βCD in bulk water and in the channel. On the contrary, the hydrogen bonds connecting adjacent glucose residues, i.e., O2···O3, stabilize significantly when βCD is located within the pore of the channel. This observation is consistent with the conformational behavior of the Ψ dihedral angle (see the previous section). Namely, conformations with Ψ > 120°, which are incompatible with such hydrogen bonds, are precluded in the channel due to the interaction with the walls of the pore. The dynamics of the angles χ_2 and χ_3 shows the flip-flop O2(i)···O3($i+1$) hydrogen bonding for βCD both in the channel and in bulk water. This hydrogen-bonding pattern was found in the crystalline βCD hydrates, e.g., βCD·12H_2O, by neutron-diffraction studies[86] and was successfully reproduced in MD simulation of crystalline βCD.[44]

Occupancies of hydrogen bonds formed by βCD with water are listed in Table 6. The number of hydrogen bonds formed by βCD with water in the channel decreases to 70% of its value in bulk water. This mainly results from the fewer water molecules available in the vicinity of βCD in the pore and also from the competing hydrogen bonds with the side chains of the protein. In the systems A45, A50, B45, and B50 the possible hydrogen bonds of βCD with the protein involve hydroxyl groups of Thr115 and Thr145 (Table 7). The average number of all possible hydrogen bonds between Thr115, Thr145 and βCD is about 3. Few direct hydrogen bonds observed in the simulation are consistent with observation of crystal protein−βCD structures (vide supra), where typically four hydrogen bonds were found.

The lack of direct hydrogen bonds between the guest molecule and the protein can be compensated by water-mediated hydrogen bonds. The water-mediated hydrogen bonds in the systems A45 and A50 are formed mainly between O2 and O3 atoms of βCD and the residues Thr115, Thr117, and Thr145. They are formed less frequently between O6 atoms of βCD and Lys147 side chains. The average number of these bonds is eight. A pattern of direct and water-mediated hydrogen bonds for a snapshot from the MD simulation is schematically represented in Figure 10. The binding motif for αHL−βCD interaction observed in this simulation is similar in its hydrogen-bonding pattern to that of the known crystal protein−βCD structures. However, since in the present case most hydrophobic residues of the protein

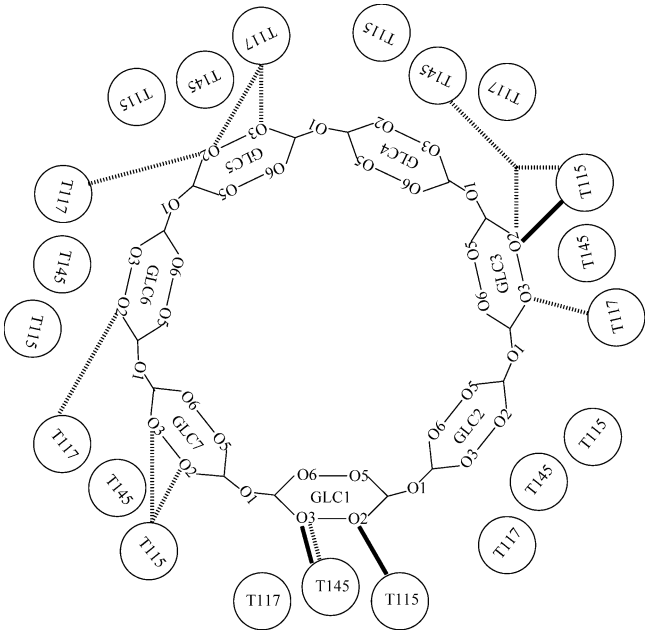

Figure 10. Schematic diagram representing direct (solid lines) and water-mediated (dotted line) hydrogen bonds between βCD and residues Thr115, Thr117, and Thr145 for the final snapshot of the system A50.

TABLE 7: Average Occupancies of Hydrogen Bonds between βCD and Thr115, Thr145, %

H-bond type (donor atom)−(hydrogen)···(acceptor atom)	A45	A50	B45	B50
(Thr-115 OG1)−(Thr-115 HG1)···(βCD O2)	4.7	7.0	2.1	0.6
(Thr-115 OG1)−(Thr-115 HG1)···(βCD O3)	0.4	3.8	3.7	2.3
(Thr-115 OG1)−(Thr-115 HG1)···(βCD O5)	0.6	0.2	0.5	0.6
(Thr-115 OG1)−(Thr-115 HG1)···(βCD O6)	0.2	0.4	2.5	0.4
(βCD O2)−(βCD HO2)···(Thr-115 OG1)	6.4	10.0	1.3	0.5
(βCD O3)−(βCD HO3)···(Thr-115 OG1)	2.9	3.8	6.2	6.0
(βCD O6)−(βCD HO6)···(Thr-115 OG1)	7.5	3.1	2.3	4.4
(Thr-145 OG1)−(Thr-145 HG1)···(βCD O2)	0.0	1.2	5.1	12.2
(Thr-145 OG1)−(Thr-145 HG1)···(βCD O3)	2.2	2.1	1.2	0.1
(Thr-145 OG1)−(Thr-145 HG1)···(βCD O5)	0.0	0.3	0.1	0.1
(Thr-145 OG1)−(Thr-145 HG1)···(βCD O6)	7.2	3.8	0.8	0.0
(βCD O2)−(βCD HO2)···(Thr-145 OG1)	0.2	1.2	15.2	21.6
(βCD O3)−(βCD HO3)···(Thr-145 OG1)	1.3	5.7	5.5	0.7
(βCD O6)−(βCD HO6)···(Thr-145 OG1)	1.5	3.7	3.6	0.0

β-barrel are oriented toward the membrane, there are no stacking interactions with aromatic side chains. Such interactions were observed in most other hydrocarbon-protein complexes. As seen in Figure 11, the binding motif does not follow the 7-fold symmetry of βCD and the surrounding protein, indicating a geometric mismatch due to conformational motion as well as weak binding affinity.

4. Conclusions

In this study, we performed a series of MD simulations of β-cyclodextrin within the channel formed by the α-hemolysin protein. A total of 10 starting geometries with different positions and orientations of β-cyclodextrin inside the channel lumen were used to explore the range of possible configurations of βCD when it penetrates the pore. The experimental residence time of βCD within the channel varied in the range 0.1−3 ms with the mean value 0.7 ms.[21] Thus, the whole process of the movement of βCD in the interior of the channel, including diffusion to a binding site, binding, subsequent unbinding, and diffusion in the backward direction has the millisecond time scale and is beyond the scope of conventional molecular dynamics simulation. Note that the time scale of complex formation between αHL and βCD is similar to that of gating transitions in ion channels, which often occur over several milliseconds.[87] Although the overall simulation time was long by the standards of MD simulations it was substantially shorter than the expected time of the diffusion of βCD molecule inside the channel pore. The sampling of starting positions along the channel axis helped compensate for the insufficient time of the simulation and allowed us to investigate the channel−βCD interactions along the length of the channel. A number of configurations were identified as probable binding states, and insights into dynamics of βCD on the nanosecond time scale were obtained. The simulation of βCD in bulk water was also performed. We provided a detailed analysis of the interaction energetics and conformational flexibility of βCD inside the water−protein channel, carefully elucidating the intra- and intermolecular hydrogen bonding in the complex and in aqueous solution and discussed the implications of the confined environment on the dynamics of the cyclodextrin molecule.

The simulation revealed a number of binding states characterized by different binding affinities. The equilibrated configurations with βCD residing in the vicinity of Met113 with its wider rim oriented toward the trans side of the membrane were found to be the most favorable in terms of both interaction and binding free energies. Although both methods took into account only a limited number of possible contributions, the predicted location of the most stable binding site is in agreement with conclusions from the indirect experimental results. The favorable contributions to the binding affinity are the van der Waals interactions between αHL and βCD and the nonpolar solvation effects. The binding is characterized by the van der Waals contacts with Met113, Thr115, and Thr145 and electrostatic interactions with Glu111 and Lys147. Hydrogen-bonding pattern comprises few direct bonds with Thr115, Thr145 and several water-mediated hydrogen bonds with Thr115, Thr117, Thr145, and Lys147. Mutation of these residues, except Met113, which has already been studied systematically, is expected to alter the binding affinity to βCD.

Conformational flexibility of the macroring of βCD was found to be considerably reduced by confined environment of the channel, although its overall shape remained unchanged upon entering the channel. The conformational motion of side groups of αHL at the binding site was also affected in the vicinity of βCD. However, only a few torsion angles in both βCD and αHL side chains exhibited a significant change in their equilibrium distributions upon binding. These findings provide structural and energetic insights into mechanisms of protein−carbohydrate interactions and can be taken into account in developing stochastic sensors based on αHL ion channel. Our analysis also provides important information needed to construct a more "coarse-grained" model for the αHL−βCD interactions, which will allow the direct simulation of stochastic binding process in the further work.

Acknowledgment. Funding for this work was provided by Marquette University. The authors thank H. Bayley and L.-Q. Gu for valuable discussions.

References and Notes

(1) Toone, E. J.; Burkhalter, N. F.; Dimick, S. M. *Carbohydr. Chem. Biol.* **2000**, *2*, 863−914.
(2) Toone, E. J. *Curr. Opin. Struct. Biol.* **1994**, *4*, 719−728.
(3) Weis, W. I.; Drickamer, K. *Annu. Rev. Biochem.* **1996**, *65*, 441−473.
(4) Dam, T. K.; Brewer, C. F. *Chem. Rev.* **2002**, *102*, 387−429.
(5) Dwek, R. A. *Chem. Rev.* **1996**, *96*, 683−720.
(6) Lis, H.; Sharon, N. *Chem. Rev.* **1998**, *98*, 637−674.
(7) Lee, Y. C.; Lee, R. T. *Acc. Chem. Res.* **1995**, *28*, 321−327.
(8) Sharon, N.; Ofek, I. *Glycoconjugate J.* **2000**, *17*, 659−664.

(9) Nangia-Makker, P.; Conklin, J.; Hogan, V.; Raz, A. *Trends Mol. Med.* **2002**, *8*, 187−192.
(10) Davis, A. P.; Wareham, R. S. *Angew. Chem., Int. Ed. Engl.* **1999**, *38*, 2979−2996.
(11) Lemieux, R. U. *Acc. Chem. Res.* **1996**, *29*, 373−380.
(12) Carver, J. P. *Pure Appl. Chem.* **1993**, *65*, 763−770.
(13) Szejtli, J. *Chem. Rev.* **1998**, *98*, 1743−1754.
(14) Rekharsky, M. V.; Inoue, Y. *Chem. Rev.* **1998**, *98*, 1875−1917.
(15) Hedges, A. R. *Chem. Rev.* **1998**, *98*, 2035−2044.
(16) Sorimachi, K.; Gal-Coeffet, M. F.; Williamson, G.; Archer, D. B.; Williamson, M. P. *Structure (London)* **1997**, *5*, 647−661.
(17) Adachi, M.; Mikami, B.; Katsube, T.; Utsumi, S. *J. Biol. Chem.* **1998**, *273*, 19859−19865.
(18) Sharff, A. J.; Rodseth, L. E.; Quiocho, F. A. *Biochemistry* **1993**, *32*, 10553−10559.
(19) Kondo, S.; Ohtaki, A.; Tonozuka, T.; Sakano, Y.; Kamitori, S. *J. Biochem.(Tokyo)* **2001**, *129*, 423−428.
(20) Yokota, T.; Tonozuka, T.; Shimura, Y.; Ichikawa, K.; Kamitori, S.; Sakano, Y. *Biosci., Biotechnol., Biochem.* **2001**, *65*, 619−626.
(21) Gu, L.-Q.; Bayley, H. *Biophys. J.* **2000**, *79*, 1967−1975.
(22) Gu, L.-Q.; Serra, M. D.; Vincent, J. B.; Vigh, G.; Cheley, S.; Braha, O.; Bayley, H. *Proc. Natl. Acad. Sci. U.S.A.* **2000**, *97*, 3959−3964.
(23) Gu, L.-Q.; Braha, O.; Conlan, S.; Cheley, S.; Bayley, H. *Nature (London)* **1999**, *398*, 686−690.
(24) Gu, L.-Q.; Cheley, S.; Bayley, H. *Science (Washington, D.C.)* **2001**, *291*, 636−640.
(25) Gu, L.-Q.; Cheley, S.; Bayley, H. *J. Gen. Physiol.* **2001**, *118*, 481−494.
(26) Hansson, T.; Oostenbrink, C.; van Gunsteren, W. F. *Curr. Opin. Struct. Biol.* **2002**, *12*, 190−196.
(27) Roux, B. *Curr. Opin. Struct. Biol.* **2002**, *12*, 182−189.
(28) Tieleman, D. P.; Biggin, P. C.; Smith, G. R.; Sansom, M. S. P. *Q. Rev. Biophys.* **2001**, *34*, 473−561.
(29) Duan, Y.; Kollman, P. A. *Science (Washington, D.C.)* **1998**, *282*, 740−744.
(30) Daggett, V. *Curr. Opin. Struct. Biol.* **2000**, *10*, 160−164.
(31) Zacharias, M.; Straatsma, T. P.; McCammon, J. A.; Quiocho, F. A. *Biochemistry* **1993**, *32*, 7428−7434.
(32) Imberty, A.; Perez, S. *Glycobiology* **1994**, *4*, 351−366.
(33) Åqvist, J.; Mowbray, S. L. *J. Biol. Chem.* **1995**, *270*, 9978−9981.
(34) Liang, G.; Schmidt, R. K.; Yu, H. A.; Cumming, D. A.; Brady, J. W. *J. Phys. Chem.* **1996**, *100*, 2528−2534.
(35) Cheong, Y.; Shim, G.; Kang, D.; Kim, Y. *J. Mol. Struct.* **1999**, *475*, 219−232.
(36) Pathiaseril, A.; Woods, R. J. *J. Am. Chem. Soc.* **2000**, *122*, 331−338.
(37) Bernardi, A.; Galgano, M.; Belvisi, L.; Colombo, G. *J. Comput.-Aided Mol. Des.* **2001**, *15*, 117−128.
(38) Bryce, R. A.; Hillier, I. H.; Naismith, J. H. *Biophys. J.* **2001**, *81*, 1373−1388.
(39) Lipkowitz, K. B. *Chem. Rev.* **1998**, *98*, 1829−1873.
(40) Prabhakaran, M. *Biochem. Biophys. Res. Commun.* **1991**, *178*, 192−197.
(41) Lipkowitz, K. B. *J. Org. Chem.* **1991**, *56*, 6357−6367.
(42) Kozar, T.; Venanzi, C. A. *THEOCHEM* **1997**, *395*−*396*, 451−468.
(43) Wertz, D. A.; Shi, C. X.; Venanzi, C. A. *J. Comput. Chem.* **1992**, *13*, 41−56.
(44) Koehler, J. E. H.; Saenger, W.; Van Gunsteren, W. F. *Eur. Biophys. J.* **1988**, *16*, 153−168.
(45) Linert, W.; Margl, P.; Renz, F. *Chem. Phys.* **1992**, *161*, 327−338.
(46) Barbiric, D. J.; de Rossi, R. H.; Castro, E. A. *THEOCHEM* **2001**, *537*, 235−243.
(47) Fronza, G.; Mele, A.; Redenti, E.; Ventura, P. *J. Org. Chem.* **1996**, *61*, 909−914.
(48) Ivanov, P. M.; Salvatierra, D.; Jaime, C. *J. Org. Chem.* **1996**, *61*, 7012−7017.
(49) Dodziuk, H.; Lukin, O.; Nowinski, K. S. *THEOCHEM* **2000**, *503*, 221−230.
(50) Salvatierra, D.; Sanchez-Ruiz, X.; Garduno, R.; Cervello, E.; Jaime, C.; Virgili, A.; Sanchez-Ferrando, F. *Tetrahedron* **2000**, *56*, 3035−3041.
(51) Yeh, I.-C.; Hummer, G. *J. Am. Chem. Soc.* **2002**, *124*, 6563−6568.
(52) Lichtenthaler, F. W.; Immel, S. *Liebigs Ann.* **1996**, 27−37.
(53) Gouaux, E. *J. Struct. Biol.* **1998**, *121*, 110−122.
(54) Song, L.; Hobaugh, M. R.; Shustak, C.; Cheley, S.; Bayley, H.; Gouaux, J. E. *Science (Washington, D.C.)* **1996**, *274*, 1859−1866.
(55) Pearlman, D. A.; Case, D. A.; Caldwell, J. W.; Ross, W. S.; Cheatham, T. E. I.; DeBolt, S.; Ferguson, D.; Seibel, G.; Kollman, P. *Comput. Phys. Commun.* **1995**, *91*, 1−42.
(56) Cornell, W. D.; Cieplak, P.; Bayly, C. I.; Gould, I. R.; Merz, K. M., Jr.; Ferguson, D. M.; Spellmeyer, D. C.; Fox, T.; Caldwell, J. W.; Kollman, P. A. *J. Am. Chem. Soc.* **1995**, *117*, 5179−5197.
(57) Glennon, T. M.; Zheng, Y.-J.; LeGrand, S. M.; Shutzberg, B. A.; Merz, K. M., Jr. *J. Comput. Chem.* **1994**, *15*, 1019−1040.
(58) Mamonov, A.; Coalson, R. D.; Nitzan, A.; Kurnikova, M. G. *Biophys. J.* **2003**, *84*, 3646−3661.
(59) Wu, Y.; He, K.; Ludtke, S. J.; Huang, H. W. *Biophys. J.* **1995**, *68*, 2361−2369.
(60) Jorgensen, W. L.; Chandrasekhar, J.; Madura, J. D.; Impey, R. W.; Klein, M. L. *J. Chem. Phys.* **1983**, *79*, 926−935.
(61) Berendsen, H. J. C.; Postma, J. P. M.; Van Gunsteren, W. F.; DiNola, A.; Haak, J. R. *J. Chem. Phys.* **1984**, *81*, 3684−3690.
(62) Essmann, U.; Perera, L.; Berkowitz, M. L.; Darden, T.; Lee, H.; Pedersen, L. G. *J. Chem. Phys.* **1995**, *103*, 8577−8593.
(63) Ryckaert, J. P.; Ciccotti, G.; Berendsen, H. J. C. *J. Comput. Phys.* **1977**, *23*, 327−341.
(64) McQuarrie, D. A. *Statistical mechanics*; Harper & Row Publishers: New York, 1976.
(65) Allen, M. P.; Tildesley, D. J. *Computer simulation of liquids*;Oxford University Press: Oxford, England, 1987; p 450.
(66) Leach, A. R. *Molecular modelling: principles and applications*, 2nd ed.; Prentice Hall: Harlow, England, and Reading, MA, 2001.
(67) Gilson, M. K.; Honig, B. *Proteins: Struct., Funct., Genet.* **1988**, *4*, 7−18.
(68) Kurnikova, M. G.; Coalson, R. D.; Graf, P.; Nitzan, A. *Biophys. J.* **1999**, *76*, 642−656.
(69) Lee, B.; Richards, F. M. *J. Mol. Biol.* **1971**, *55*, 379−400.
(70) Le Grand, S. M.; Merz, Jr.; Kenneth, M. *J. Comput. Chem.* **1993**, *14*, 349−352.
(71) Still, W. C.; Tempczyk, A.; Hawley, R. C.; Hendrickson, T. *J. Am. Chem. Soc.* **1990**, *112*, 6127−6129.
(72) Paduano, L.; Sartorio, R.; Vitagliano, V.; Costantino, L. *J. Solution Chem.* **1990**, *19*, 31−39.
(73) Kollman, P. A.; Massova, I.; Reyes, C.; Kuhn, B.; Huo, S.; Chong, L.; Lee, M.; Lee, T.; Duan, Y.; Wang, W.; Donini, O.; Cieplak, P.; Srinivasan, J.; Case, D. A.; Cheatham, T. E. I. *Acc. Chem. Res.* **2000**, *33*, 889−897.
(74) Jayaram, B.; McConnell, K.; Dixit, S. B.; Das, A.; Beveridge, D. L. *J. Comput. Chem.* **2002**, *23*, 1−14.
(75) Noskov, S. Y.; Lim, C. *Biophys. J.* **2001**, *81*, 737−750.
(76) Sigurskjold, B. W.; Christensen, T.; Payre, N.; Cottaz, S.; Driguez, H.; Svensson, B. *Biochemistry* **1998**, *37*, 10446−10452.
(77) Thomson, J.; Liu, Y.; Sturtevant, J. M.; Quiocho, F. A. *Biophys. Chem.* **1998**, *70*, 101−108.
(78) Kuhn, B.; Kollman, P. A. *J. Med. Chem.* **2000**, *43*, 3786−3791.
(79) Reyes, C. M.; Kollman, P. A. *J. Mol. Biol.* **2000**, *297*, 1145−1158.
(80) Åqvist, J.; Luzhkov, V. B.; Brandsdal, B. O. *Acc. Chem. Res.* **2002**, *35*, 358−365.
(81) Blokzijl, W.; Engberts, J. B. F. N. *Angew. Chem., Int. Ed. Engl.* **1993**, *32*, 1545−1579.
(82) Gallicchio, E.; Kubo, M. M.; Levy, R. M. *J. Am. Chem. Soc.* **1998**, *120*, 4526−4527.
(83) Saenger, W.; Jacob, J.; Gessler, K.; Steiner, T.; Hoffmann, D.; Sanbe, H.; Koizumi, K.; Smith, S. M.; Takaha, T. *Chem. Rev.* **1998**, *98*, 1787−1802.
(84) Quiocho, F. A. *Pure Appl. Chem.* **1989**, *61*, 1293−1306.
(85) Skrynnikov, N. R.; Goto, N. K.; Yang, D.; Choy, W. Y.; Tolman, J. R.; Mueller, G. A.; Kay, L. E. *J. Mol. Biol.* **2000**, *295*, 1265−1273.
(86) Betzel, C.; Saenger, W.; Hingerty, B. E.; Brown, G. M. *J. Am. Chem. Soc.* **1984**, *106*, 7545−7557.
(87) Hille, B. *Ionic channels of excitable membranes*, 3rd ed.; Sinauer: Sunderland, MA, 2001.
(88) Sayle, R. A.; Milner-White, E. J. *Trends Biochem. Sci.* **1995**, *20*, 374−376.
(89) Klug, C. S.; Su, W.; Feix, J. B. *Biochemistry* **1997**, *36*, 13027−13033.

(90) The limited dynamics of the protein backbone in the beta-barrel has been demonstrated in the experiment, e.g., ref 89, and indirectly, in the theoretical study of ion current through the porin protein in which modeling by the all-atom MD simulation and by Brownian dynamics simulation of ions in the rigid protein gave very similar distributions of ions inside the channel indicating that the dynamics of the protein backbone is unimportant for the dynamics inside the pore.[27] In the current study, we are interested in the dynamics of the ligand molecule inside the pore. The β-barrel forms a well-defined barrier to separate the system into two compartments: inside the pore where we attempted to simulate the all-atom dynamics of all species involved in full detail and behind the barrel wall, where simplified constrained dynamics of the model lipid bilayer, protein backbone was employed because the influence of this region onto the dynamics inside the pore is expected to be small.